HAL
open science

Cardiopharyngeal mesoderm origins of musculoskeletal and connective tissues in the mammalian pharynx

Noritaka Adachi, Marchesa Bilio, Antonio Baldini, Robert G Kelly

To cite this version:

Noritaka Adachi, Marchesa Bilio, Antonio Baldini, Robert G Kelly. Cardiopharyngeal mesoderm origins of musculoskeletal and connective tissues in the mammalian pharynx. Development (Cambridge, England), 2020, 147 (3), pp.dev185256. 10.1242/dev.185256 . hal-03142010

HAL Id: hal-03142010

https://amu.hal.science/hal-03142010v1

Submitted on 15 Feb 2021

HAL is a multi-disciplinary open access archive for the deposit and dissemination of scientific research documents, whether they are published or not. The documents may come from teaching and research institutions in France or abroad, or from public or private research centers.

L'archive ouverte pluridisciplinaire **HAL**, est destinée au dépôt et à la diffusion de documents scientifiques de niveau recherche, publiés ou non, émanant des établissements d'enseignement et de recherche français ou étrangers, des laboratoires publics ou privés.

Copyright

© 2020. Published by The Company of Biologists Ltd | Development (2020) 147, dev185256. doi:10.1242/dev.185256

RESEARCH ARTICLE

Cardiopharyngeal mesoderm origins of musculoskeletal and connective tissues in the mammalian pharynx

Noritaka Adachi[1,*], Marchesa Bilio[2], Antonio Baldini[2,3] and Robert G. Kelly[1,*]

ABSTRACT

Cardiopharyngeal mesoderm (CPM) gives rise to muscles of the head and heart. Using genetic lineage analysis in mice, we show that CPM develops into a broad range of pharyngeal structures and cell types encompassing musculoskeletal and connective tissues. We demonstrate that CPM contributes to medial pharyngeal skeletal and connective tissues associated with both branchiomeric and somite-derived neck muscles. CPM and neural crest cells (NCC) make complementary mediolateral contributions to pharyngeal structures, in a distribution established in the early embryo. We further show that biallelic expression of the CPM regulatory gene *Tbx1*, haploinsufficient in 22q11.2 deletion syndrome patients, is required for the correct patterning of muscles with CPM-derived connective tissue. Our results suggest that CPM plays a patterning role during muscle development, similar to that of NCC during craniofacial myogenesis. The broad lineage contributions of CPM to pharyngeal structures provide new insights into congenital disorders and evolution of the mammalian pharynx.

KEY WORDS: CPM, Neural crest cells, Pharyngeal arch, Pharynx, Tbx1, 22q11.2 deletion syndrome, Mouse

INTRODUCTION

The pharynx is essential for feeding, breathing and speech, and the pharyngeal arches (PAs), segmental structures in the vertebrate embryo, play a crucial role in pharyngeal development. Two types of mesenchymal progenitor cells are located in the embryonic pharynx and contribute to different elements of the pharyngeal apparatus during morphogenesis.

One is neural crest cells (NCCs) that originate from the dorsal neural tube and reside peripherally in PAs. NCCs have been shown to make a crucial contribution to the vertebrate pharyngeal skeleton and also give rise to connective tissues (CTs) of skeletal and muscular systems (Le Douarin et al., 2004; Noden and Trainor, 2005; Minoux and Rijli, 2010). NCCs further possess patterning information that dictates the morphology of musculoskeletal elements in the head (Schneider and Helms, 2003; Le Douarin et al., 2004; Noden and Trainor, 2005; Rinon et al., 2007; Tokita and Schneider, 2009; Gitton et al., 2010). NCCs are therefore postulated to have a pivotal role in the development and evolution of the vertebrate head and pharyngeal apparatus. Nevertheless, mutant analyses of Hox and Dlx genes that are expressed in NCCs have failed to show a clear homeotic transformation in posterior PA derivatives, unlike jaw and ear elements derived from anterior PAs (Beverdam et al., 2002; Depew et al., 2002; Minoux et al., 2009; Minoux and Rijli, 2010).

The other key component in pharyngeal development is cardiopharyngeal mesoderm (CPM), a subset of head mesoderm in the embryonic pharynx. CPM yields pharyngeal mesoderm in the core of the PAs and second heart field (SHF) cardiac progenitor cells, and contributes to several lineages, including skeletal muscles in the head and neck, SHF-derived cardiac elements and cervical arteries (Kelly et al., 2001; Lescroart et al., 2010, 2015; Gopalakrishnan et al., 2015; Diogo et al., 2015; Wang et al., 2017). Indispensable genes and markers for CPM development include *Isl1*, and *Fgf10* and *Mef2c* enhancer transgenes (Kelly et al., 2001; Cai et al., 2003; Verzi et al., 2005). The gene encoding the T-box containing transcription factor, *Tbx1*, is also expressed in CPM. *TBX1* is the major gene for 22q11.2 deletion syndrome (22q11.2DS, also known as DiGeorge or Velocardiofacial syndrome), characterized by a spectrum of defects in craniofacial, pharyngeal and cardiovascular structures (Jerome and Papaioannou, 2001; Lindsay et al., 2001; Merscher et al., 2001; Yagi et al., 2003). *Tbx1* plays an upstream role in the regulatory hierarchy driving branchiomeric but not somitic myogenesis, and mice lacking *Tbx1* exhibit severe musculoskeletal defects in the head and neck region (Jerome and Papaioannou, 2001; Lindsay et al., 2001; Merscher et al., 2001; Kelly et al., 2004; Dastjerdi et al., 2007; Sambasivan et al., 2009; Kong et al., 2014; Heude et al., 2018).

The view that NCCs contribute to skeletal elements and CT, while CPM gives rise to musculature during pharyngeal development has been challenged by evidence for a mesodermal origin of components of the pharyngeal skeleton and CT in amniotes (Noden, 1988; Tabler et al., 2017; Heude et al., 2018). In these studies, however, the lateral mesoderm (mesoderm adjacent to the otic vesicle and the first somite) was traced in chicken-quail chimera analysis, and *Mesp1-Cre* mice, labeling anterior somites, lateral plate mesoderm (LPM) and head mesoderm, were employed in genetic lineage analysis. Therefore, the precise mesodermal origins of the pharyngeal skeleton and CT remain elusive. Given the genetic differences between head and trunk mesoderm, the identification of mesodermal sources of pharyngeal structures is essential to understand the development, pathology and evolution of the pharynx (Buckingham and Vincent, 2009; Sambasivan et al., 2011).

Here, we have mapped the contribution of CPM to pharyngeal structures by genetic lineage tracing using *Mef2c* gene Anterior Heart Field enhancer (*Mef2c-AHF-Cre*) and *Rosa26*$^{Stop/YFP}$ (yellow fluorescent protein, hereafter called *RYFP*) transgenic mice (Srinivas et al., 2001; Verzi et al., 2005). *Mef2c-AHF-Cre* drives *Cre* expression in CPM including head muscle progenitor cells and the SHF (Verzi et al., 2005). By comparison with genetic lineage

[1]Aix-Marseille Université, CNRS UMR 7288, IBDM, 13009 Marseille, France. [2]CNR Institute of Genetics and Biophysics Adriano Buzzati-Traverso, Via Pietro Castellino 111, 80131 Naples, Italy. [3]Department of Molecular Medicine and Medical Biotechnology, University of Naples Federico II, Naples 80131, Italy.

*Authors for correspondence (adaraptor@gmail.com; Robert.Kelly@univ-amu.fr)

N.A., 0000-0002-9482-8436; R.G.K., 0000-0003-4357-0073

Received 2 October 2019; Accepted 16 December 2019

Development (2020) 147, dev185256. doi:10.1242/dev.185256

analysis of NCC derivatives, and validation with *Tbx1-Cre*, a second *Cre* line expressed in CPM (Huynh et al., 2007), we demonstrate that CPM contributes to a broader spectrum of posterior pharyngeal structures than had been previously thought, including cartilage and CT. The latter fate implies a potential role for CPM in muscle patterning, reinforced by the identification of neck muscle patterning defects in mice that are haploinsufficient for the CPM regulatory gene *Tbx1*. By highlighting the major contribution of CPM, our results bring new clinical and evolutionary insights into development of the mammalian pharyngeal apparatus.

RESULTS

Specificity of the *Mef2c-AHF-Cre* line for CPM labeling

In order to investigate the contribution of the *Mef2c-AHF-Cre* genetic lineage to pharyngeal structures, we first assessed the specificity of genetic labeling by *Mef2c-AHF-Cre* at embryonic day (E)15.5. At this stage, musculoskeletal elements are well developed and identifiable in histological sections (Kaufman, 1992). We used immunofluorescence to detect YFP labeling in *Mef2c-AHF-Cre; RYFP* mice that identifies *Cre*-expressing cells and their descendants. Consistent with previous results, we observed YFP$^+$ cells in PA-derived skeletal muscles (Figs S1 and S2) (Lescroart et al., 2010; Lescroart et al., 2015; Heude et al., 2018). In addition to branchiomeric muscles, YFP$^+$ cells were found in PA artery derivatives including the carotid arteries and in the myocardium of the outflow tract and right ventricle (Fig. S2) (Verzi et al., 2005; Wang et al., 2017). In contrast, NCC, LPM and somitic derivatives, as well as ectodermal and endodermal structures, were YFP-negative (see details in Figs S1 and S2) (Köntges and Lumsden, 1996; Chai et al., 2000; Jiang et al., 2000; Huang et al., 2000; Le Douarin et al., 2004; Noden and Trainor, 2005; Matsuoka et al., 2005; Heude et al., 2018). Consistent with these results, activation of *Cre* or *Mef2c-AHF-Cre* derivatives has not been observed in NCCs, LPM, somite, ectoderm or endoderm for this transgenic line during early development (from E7.5 to E12.5; this study; Verzi et al., 2005; Lescroart et al., 2015). Collectively, these results confirm the expression of *Mef2c-AHF-Cre* in CPM and validate the use of this line to genetically trace the contribution of CPM to the pharyngeal region.

CPM gives rise to skeletal structures and mesenchyme in the pharynx and shoulder

Analysis of transverse sections at pharyngeal and shoulder levels revealed that skeletal components were labeled in the *Mef2c-AHF-Cre* line. Arytenoid, cricoid and tracheal cartilages, as well as the mid-ventral portion of the thyroid cartilage, were YFP$^+$ (Fig. 1A-H). However, the dorsal and lateral parts of the thyroid cartilage were devoid of YFP$^+$ cells. At the shoulder level, the medial portion of the clavicle and the dorsal end of the sternum were specifically labeled by YFP (Fig. 1E,H), whereas the lateral part of the clavicle and the ventral sternum were YFP$^-$ (Fig. S2F,K).

Close analysis of sections revealed that YFP$^+$ cells were distributed in the cell layer surrounding pharyngeal and shoulder skeletons. These perichondrial cells were detected around arytenoid, cricoid and tracheal cartilages (Fig. 1, Fig. S3). The perichondrium of the mid-ventral thyroid cartilage was also YFP$^+$,

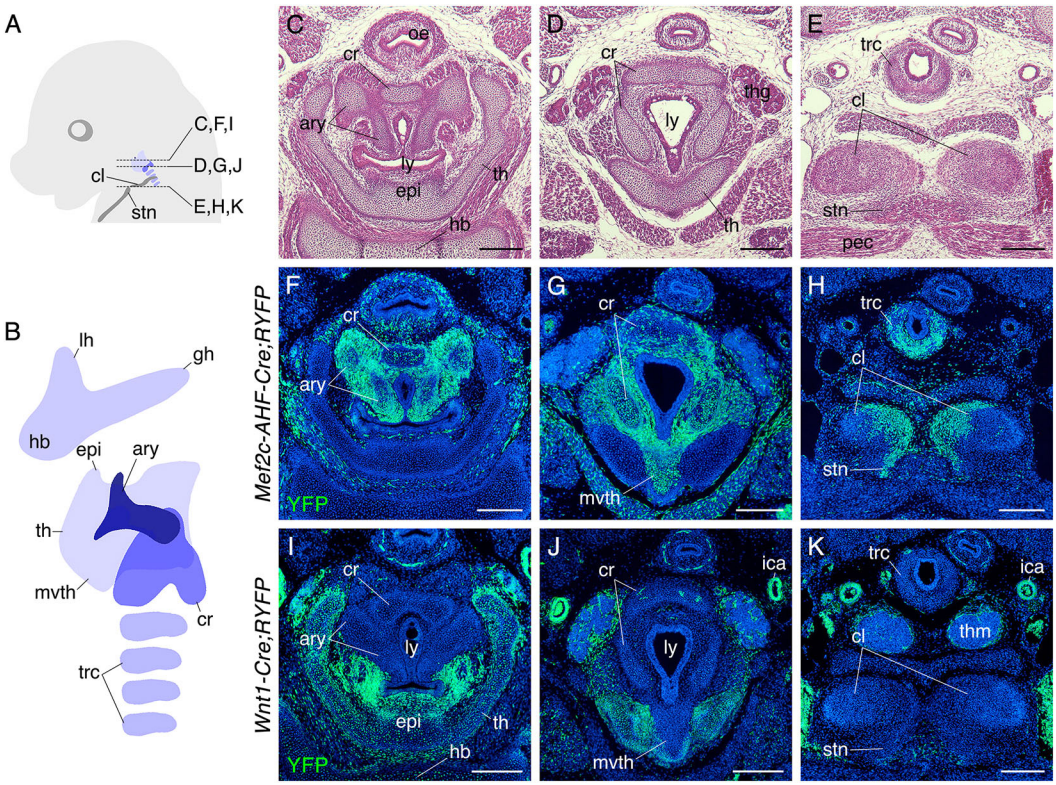

Fig. 1. CPM origins of pharyngeal and shoulder skeletons. (A,B) Diagrams of a mouse embryo showing the transverse section levels of panels C to K (A) and pharyngeal skeletal elements (B). (C-E) Hematoxylin and Eosin (H&E) staining of sections at E15.5. (F-H) YFP immunostaining of *Mef2c-AHF-Cre;RYFP* sections at E15.5 showing labeling in skeletal components of the pharynx and shoulder (*n*=7). (I-K) YFP immunostaining of *Wnt1-Cre;RYFP* sections at E15.5 showing the complementary distribution of NCCs and CPM (*n*=4). ary, arytenoid cartilage; cl, clavicle; cr, cricoid cartilage; epi, epiglottis; gh, greater horn of hyoid bone; hb, hyoid bone; ica, internal carotid artery; lh, lesser horn of hyoid bone; ly, laryngeal endoderm; mvth, mid-ventral part of thyroid cartilage; oe, oesophagus; pec, pectoralis; stn, sternum manubrium; th, thyroid cartilage; thg, thyroid gland; thm, thymus; trc, tracheal cartilage. Scale bars: 200 µm.

Development (2020) 147, dev185256. doi:10.1242/dev.185256

whereas that of the lateral portions of the thyroid cartilage was YFP^{-}. In addition, the medial perichondrium of the clavicle was marked by YFP. The distribution of labeled CT thus matches the contribution of the *Mef2c-AHF-Cre* genetic lineage to cartilaginous and bony elements in the pharyngeal and neck region. In addition to skeletal and perichondrial cells, we found *Mef2c-AHF-Cre* derivatives in medial pharyngeal mesenchyme. YFP^{+} cells were distributed in mesenchymal cells around esophageal and laryngeal endoderm, and also detected adjacent to the thyroid gland (Fig. 1F-H, Fig. S3C-E′). Together, these analyses demonstrate that CPM expressing the *Mef2c-AHF-Cre* transgene contributes to medial skeletons, skeletal CT and mesenchymal cells in the pharynx and shoulder.

To compare the *Mef2c-AHF-Cre* genetic lineage with sites of active transgene expression, we next evaluated *Cre* activity at E15.5 using *in situ* hybridization. Whereas *Cre* expression was observed in the outlet region of the heart, where the *Mef2c-AHF* enhancer was shown previously to be active at fetal stages (Verzi et al., 2005), expression was undetectable in other tissues (Fig. S4). These results are consistent with downregulation of *Mef2c-AHF-Cre* expression in the right ventricle and venous pole myocardial progenitor cells in the posterior CPM (Verzi et al., 2005; Goddeeris et al., 2008; De Bono et al., 2018). YFP labeling in visceral and shoulder skeletal elements, as well as perichondrial and mesenchymal cells, is thus likely to be the result of recombination events at earlier developmental stages, rather than *de novo* expression of *Cre* in these structures at the time of observation.

As NCCs have been proposed to contribute to the pharyngeal skeleton, we further performed a lineage analysis using *Wnt1-Cre;RYFP* mice, which genetically label NCCs in PAs and their descendants. NCC derivatives were found in the hyoid bone, epiglottis, thyroid cartilage, cranial nerves, smooth muscles of internal carotid artery and mesenchyme around the thyroid and thymus glands, consistent with previous results (Fig. 1I-K, Fig. S5) (Jiang et al., 2000; Matsuoka et al., 2005; Foster et al., 2008; Tabler et al., 2017; Heude et al., 2018). Importantly, medial skeletal components were mostly devoid of *Wnt1-Cre* lineage-positive cells, including the cricoid and arytenoid cartilages, as well as the mid-ventral thyroid cartilage (Fig. 1I,J). Similarly, *Wnt1-Cre* derivatives were sparse in the mesenchyme around the pharyngeal endoderm (Fig. 1I,J, Fig. S5). Further observations revealed a minor NCC contribution to the posterior part of the cricoid cartilage near the articulation site with the thyroid cartilage, and no overt *Wnt1-Cre* derivatives in tracheal cartilages and shoulder skeletons (Fig. 1J,K). Our results support and extend recent analyses of neural crest and mesodermal contributions to the pharyngeal skeleton (Tabler et al., 2017; Heude et al., 2018). In particular, we observed complementary medial and lateral contributions of CPM and NCC to cartilaginous elements in the pharynx and identify CPM as the source of mesodermal pharyngeal skeletal elements.

CPM contributes to muscle connective tissue in the pharynx and neck

The observation that CPM contributes to skeletal CT led us to investigate whether CPM also contributes to the CT of pharyngeal muscles. *Mef2c-AHF-Cre* derivatives were detected in the myofibers of laryngeal muscles (lcary, thary and vm in Fig. 2B),

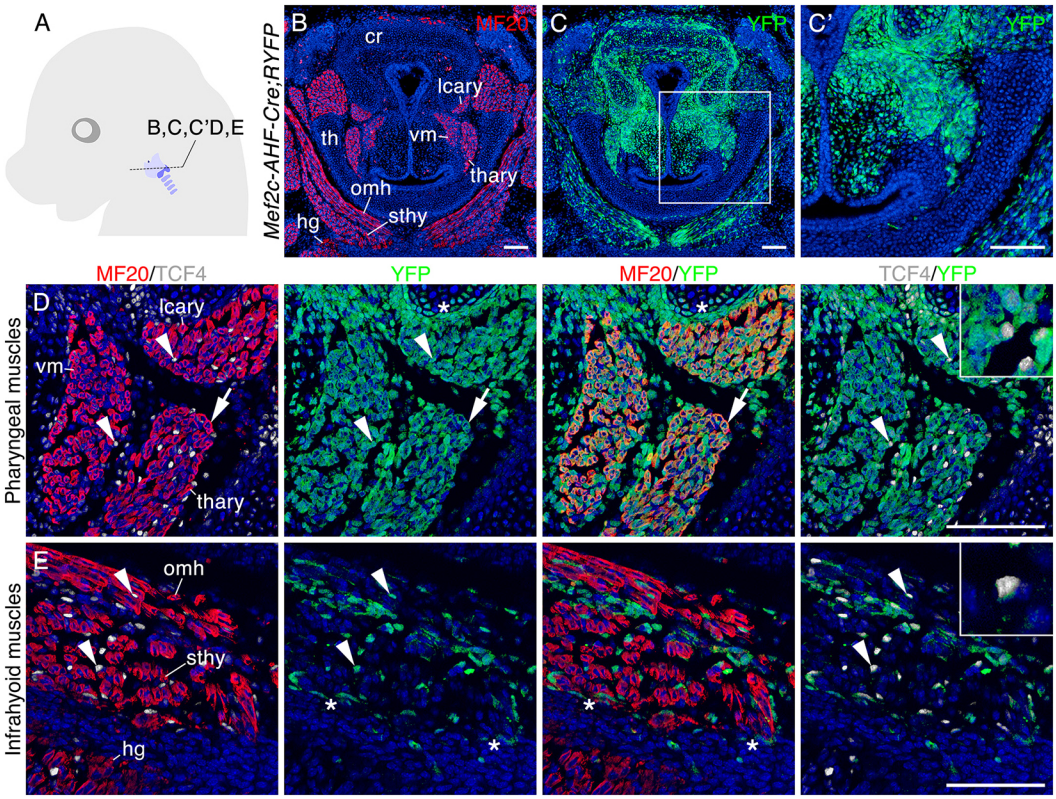

Fig. 2. CPM origins of CT in pharyngeal and infrahyoid muscles. (A) Diagram showing the section level of panels B to E. (B,C) MF20 (B) and YFP (C) immunostaining of *Mef2c-AHF-Cre;RYFP* sections at E15.5 (*n*=7). (C′) Magnification of the boxed area in C. (D,E) MF20, TCF4 and YFP immunostaining in pharyngeal (D) and infrahyoid (E) muscles (*n*=6). Co-localization of MF20/YFP (arrows) and TCF4/YFP (arrowheads, magnified in insets), and YFP signals at the muscle attachment site (asterisks) are indicated. cr, cricoid cartilage; hg, hyoglossus muscle; lcrary, lateral cricoarytenoid muscle; omh, omohyoid muscle; sthy, sternohyoid muscle; th, thyroid cartilage; thary, thyroarytenoid muscle; vm, vocal muscle. Scale bars: 100 µm.

Development (2020) 147, dev185256. doi:10.1242/dev.185256

consistent with their branchiomeric as opposed to somitic mesodermal origin (Fig. 2A-C) (Lescroart et al., 2015; Tabler et al., 2017). However, we observed that YFP labeling in these muscles was denser than that of MF20, a myosin heavy chain antibody labeling myofibers, suggesting that YFP$^+$ cells contribute to both muscle cells and surrounding muscle CT (MCT) (Fig. 2B-C′). To further investigate this, we used an anti-TCF4 antibody to identify MCT progenitor cells (Kardon et al., 2003). Analysis at single cell resolution revealed co-localization of YFP and MF20 in myofibers, and YFP and TCF4 in surrounding MCT (Fig. 2D). A similar contribution of the *Mef2c-AHF-Cre* lineage to both myofibers and MCT was also noted in other pharyngeal and laryngeal muscles, and notably YFP$^+$ MCT cells were observed in the medial portion of the cricothyroid and sternocleidomastoid muscles (Fig. S6A). Moreover, the attachment sites of pharyngeal muscles to arytenoid and cricoid cartilages were labeled by YFP (Fig. 2B-D, Fig. S6A).

Unexpectedly, we also detected *Mef2c-AHF-Cre* derivatives in MCT associated with infrahyoid muscles (omh and sthy in Fig. 2B,C). Infrahyoid neck muscles are non-branchiomeric muscles originating in the somites that migrate secondarily into the neck region as part of the hypoglossal cord (Mackenzie et al., 1998; Noden and Trainor, 2005; Heude et al., 2018). Co-immunostaining showed that, although the *Mef2c-AHF-Cre* genetic lineage does not contribute to MF20$^+$ muscle fibers in these muscles, YFP$^+$ cells co-localized with TCF4 (Fig. 2E). YFP$^+$ MCT was also found in other infrahyoid muscles, and notably at the attachment site of infrahyoid muscles to the body of the hyoid bone (Fig. 2C,E, Fig. S6B). In contrast, somite-derived tongue muscles, including the hyoglossus, that are derived from more anterior regions of the hypoglossal cord, were devoid of YFP$^+$ TCF4$^+$ MCT (Fig. 2E). As in the case of skeletal elements, *in situ* hybridization revealed that these sites of *Mef2c-AHF-Cre*-activated YFP expression are not sites of active *Cre* expression at E15.5 (Fig. S4). This suggests that YFP labeling in MCT results from genetic lineage tracing of cells expressing *Cre* at earlier developmental stages.

NCCs are considered to be a major source of MCT in pharyngeal and infrahyoid muscles (Köntges and Lumsden, 1996; Le Douarin et al., 2004; Noden and Trainor, 2005; Matsuoka et al., 2005). Our analysis of *Wnt1-Cre;RYFP* embryos showed that NCCs contribute to MCT in the lateral, but not medial, component of pharyngeal muscles, such as the cricothyroid muscle, in which MCT is predominantly derived from *Wnt1-Cre*$^+$ cells (Fig. 3A-C,G-I, Fig. S5A-D″). In contrast, MCT in the medial component of these muscles was derived from *Mef2c-AHF-Cre*-expressing progenitor cells, revealing a strikingly complementary contribution of the two sources of MCT to different regions of individual muscles (Fig. 3D-I). Dual cellular origins of MCT was also observed in somitic infrahyoid muscles, however only very few NCC-derived cells were associated with these muscles, with the exception of the thyrohyoid muscle (Fig. S5C-E″). In summary, CPM gives rise to MCT of both branchiomeric-derived pharyngeal and somitic-derived infrahyoid muscles, and makes a complementary contribution to that of NCC-derived MCT.

Unique distribution of CPM, NCC and myoblasts in the posterior PAs

The above observations demonstrate that CPM gives rise to medial skeletal elements and CT proximal to pharyngeal endoderm, whereas NCCs contribute to more lateral components in the pharynx (Figs 1–3). Considering that the typical PA configuration is a central CPM core surrounded by peripheral NCCs adjacent to pharyngeal ectoderm and endoderm, the above cellular distribution is unusual, potentially arising by remodeling of PA mesenchyme

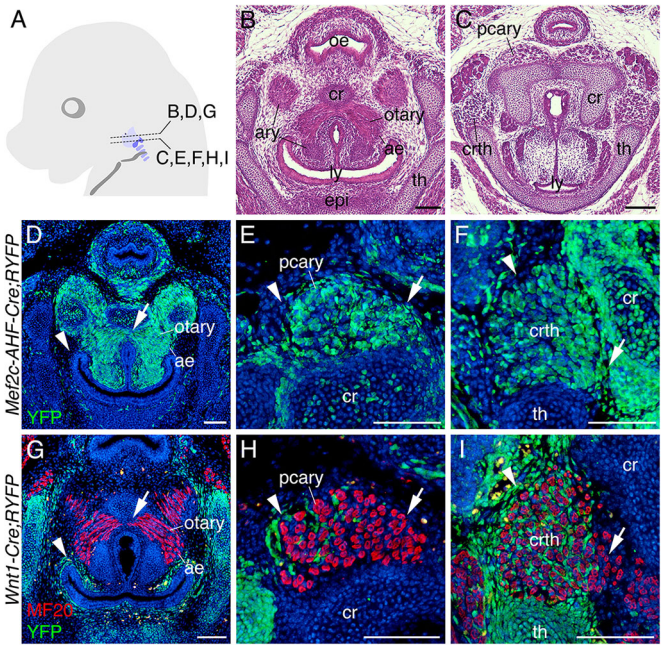

Fig. 3. The complementary mediolateral distribution of CPM and NCC derivatives in the CT of pharyngeal muscles. (A) Diagram showing the transverse section levels of panels B to I. (B,C) H&E staining of sections at E15.5. (D-I) *Mef2c-AHF-Cre;RYFP* (*n*=7) (D-F) and *Wnt1-Cre;RYFP* (*n*=4) (G-I) at E15.5 showing the aryepiglottic, oblique and transverse arytenoid (D,G), posterior cricoarytenoid (E,H) and cricothyroid muscles (F,I). Note that *Mef2c-AHF-Cre* derivatives are found densely distributed in the medial part of the muscles (arrows), whereas *Wnt1-Cre*$^+$ cells are found in the lateral side (arrowheads). ae, aryepiglottic muscle; ary, arytenoid cartilage; cr, cricoid cartilage; crth, cricothyroid muscle; epi, epiglottis; oe, oesophagus; otary, oblique and transverse arytenoid muscle; pcary, posterior cricoarytenoid muscle; th, thyroid cartilage. Scale bars: 100 µm.

during development. To clarify this point, we investigated the cellular distribution of CPM, NCC and myogenic progenitor cells in mid-gestation embryos.

At E10.5 at the levels of the 3rd and 4th PA, *Mef2c-AHF-Cre*-labeled CPM cells were positioned centrally and *Wnt1-Cre*-labeled NCCs peripherally in PAs. In contrast, at the 6th arch level, CPM-derivatives were positioned medially and NCC-derivatives laterally, similar to the situation at E15.5 (Fig. 4A-B′,D-E′). *Mef2c-AHF-Cre* derivatives at this level were divided into medial and lateral populations, corresponding to laryngopharyngeal and trapezius/sternocleidomastoid progenitors, respectively. *Wnt1-Cre*$^+$ cells were observed between those two populations, as well as superficially to the lateral *Mef2c-AHF-Cre*$^+$ cells. In contrast, the medial population of *Mef2c-AHF-Cre*-labeled cells were not surrounded by NCC cells (Fig. 4C,F). The unique distribution of CPM and NCC derivatives in the posterior pharyngeal region thus originates early in development.

We then investigated how CPM myogenic and CT progenitor cells are distributed in mid-gestation embryos. At E10.5, the myogenic regulatory factor MYOD (MYOD1) is expressed in both branchiomeric muscle progenitor cells originating from PA mesoderm, and somite-derived progenitor cells of the tongue and infrahyoid muscles located in the hypoglossal cord (Mackenzie et al., 1998; Kelly et al., 2004; Adachi et al., 2018). In *Mef2c-AHF-Cre;RYFP* embryos, YFP and MYOD colocalized in 6th PA myoblasts at the boundary of medial *Mef2c-AHF-Cre* lineage-positive and lateral lineage-negative populations (Fig. 5A-B″).

Development (2020) 147, dev185256. doi:10.1242/dev.185256

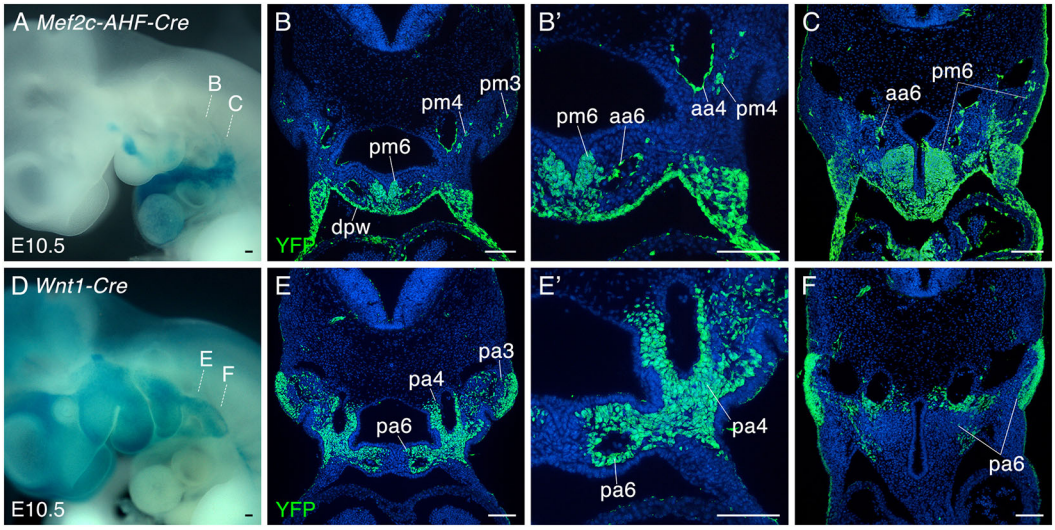

Fig. 4. The complementary mediolateral distribution of CPM and NCC in the early embryonic pharynx. (A-F) *Mef2c-AHF-Cre* (*n*=6) (A-C) and *Wnt1-Cre* (*n*=5) (D-F) embryos at E10.5 showing conditional β-galactosidase (A,D) and YFP (B-C and E-F) reporter gene expression in posterior PAs. A and D show section levels for B,C and E,F, respectively. B′ and E′ show high magnification of PAs in B and E, respectively. A unique distribution of CPM and NCCs is observed in the 6th PA. aa4-6, 4th to 6th arch artery; dpw, dorsal pericardial wall; pa3-6, 3rd to 6th pharyngeal arch; pm3-6, 3rd to 6th pharyngeal arch mesoderm. Scale bars: 100 µm.

These cells likely correspond to the progenitor cells of pharyngeal muscles with dual CPM and NCC-derived MCT contributions (Figs 2 and 3). YFP^{-} $MYOD^{+}$ cells in the posterior part of the hypoglossal cord, but not the anterior part, were enclosed by YFP^{+} mesenchymal cells (Fig. 5C-E′). This is consistent with observations that only the anterior part of the hypoglossal cord is surrounded by NCCs at E10.5 (Adachi et al., 2018). Together, these results indicate that the association of CPM with branchiomeric and somite-derived myoblasts in the posterior PA and hypoglossal cord, respectively, is established early during development. Moreover, the relative position of myoblasts and CPM at E10.5 reflects the cellular distribution of myofibers and CTs at later developmental stages, similar to the early association of CPM with NCC CT progenitor cells in anterior PAs (Noden and Trainor, 2005; Grenier et al., 2009).

The CPM regulatory gene *Tbx1* is expressed in neck muscle CT progenitor cells

The early association of NCC cells and branchiomeric muscle progenitors plays an essential role in patterning craniofacial skeletal musculature (Noden and Trainor, 2005; Rinon et al., 2007; Grenier et al., 2009). Our observations that *Mef2c-AHF-Cre* lineage-labeled cells are closely apposed to myoblasts in the posterior embryonic

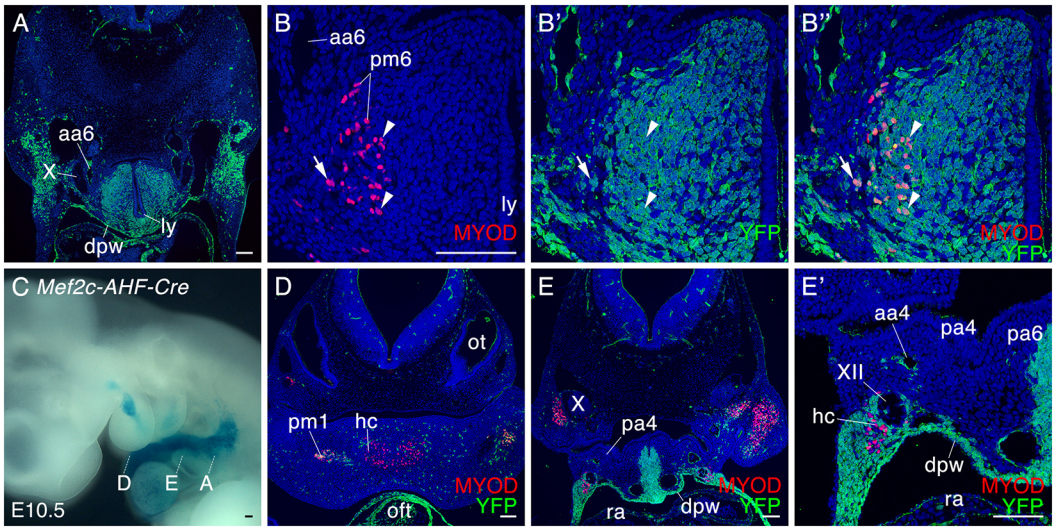

Fig. 5. Early enclosure of pharyngeal and infrahyoid myoblasts by CPM. (A-B″) YFP (A) and MYOD/YFP (B-B″) immunostaining of *Mef2c-AHF-Cre;RYFP* at E10.5 (*n*=4). The magnification of left 6th PA (B-B″) shows that some (arrowheads), but not all (arrows), $MYOD^{+}$ YFP^{+} pharyngeal myoblasts are surrounded by YFP^{+} cells. (C-E′) X-gal-stained *Mef2c-AHF-Cre;R26lacZ* embryo (C) and MYOD/YFP immunostaining of *Mef2c-AHF-Cre;RYFP* sections at E10.5 (*n*=4) (D-E′). D and E,E′ show 1st and 4th arch levels, respectively. E′ shows a high magnification of dorsal pericardium. Note that the hypoglossal cord marked by MYOD is enclosed by YFP^{+} cells at 4th arch level, but not at 1st arch level. aa4-6, 4-6th pharyngeal arch artery; dpw, dorsal pericardial wall; hc, hypoglossal cord; ly, laryngeal endoderm; oft, outflow tract; pa4-6, 4-6th pharyngeal arch; pm1-6, 1st to 6th pharyngeal arch mesoderm; ra, right atrium; X, vagus nerve; XII, hypoglossal nerve. Scale bars: 100 µm.

Development (2020) 147, dev185256. doi:10.1242/dev.185256

pharynx and give rise to MCT cells of pharyngeal and infrahyoid muscles raise the hypothesis that CPM may also play a patterning role, analogous to that of NCCs in craniofacial muscles, during pharyngeal and neck muscle development. In order to test this hypothesis we perturbed CPM development using the key CPM regulatory gene, *Tbx1*. *Tbx1* encodes a T-box containing transcription factor and is required for normal activation of the branchiomeric myogenic program and differentiation of esophageal and trapezius muscles (Kelly et al., 2004; Dastjerdi et al., 2007; Grifone et al., 2008; Sambasivan et al., 2009; Theis et al., 2010; Kong et al., 2014; Fuchs et al., 2015; Gopalakrishnan et al., 2015; Lescroart et al., 2015; Heude et al., 2018). However, a role of *Tbx1* in subsequent skeletal muscle patterning has not been described. To address this, we first examined the contribution of the *Tbx1* genetic lineage to MCT, and then characterized pharyngeal muscle patterning in heterozygous and homozygous *Tbx1* mutant embryos.

We genetically traced *Tbx1* lineages using *Tbx1-Cre;mTmG* mice [membrane-targeted tandem dimer Tomato and membrane-targeted green fluorescent protein (GFP)] embryos (Huynh et al., 2007; Muzumdar et al., 2007). Analysis at E15.5 revealed that the *Tbx1* genetic lineage gives rise to arytenoid, cricoid, mid-ventral thyroid and tracheal cartilages and their perichondrium. *Tbx1-Cre* derivatives were also detected in the clavicle and CT at muscle attachment sites on the pharyngeal skeletons, in addition to laryngeal endoderm (Fig. 6A-H). Moreover, the *Tbx1-Cre* lineage labeled branchiomeric pharyngeal and laryngeal muscles as well as TCF4$^+$ MCT cells in branchiomeric and infrahyoid muscles at E15.5 (Fig. 6F-H). In contrast to *Mef2c-AHF-Cre*, *Tbx1* has been reported to be expressed in a subset of NCC derivatives (Funato et al., 2015). However, the *Tbx1* and *Mef2c-AHF-Cre* lineages displayed highly similar labeling of *Wnt1-Cre* lineage-negative CT and, moreover, we did not observe significant GFP signal in the hyoid bone, the lateral thyroid cartilage or the lateral CT of branchiomeric muscles in which *Wnt1-Cre* derivatives were detected (Figs 1, 6 and Fig. S5). Analysis at E10.5 revealed that TBX1 was detected in cells surrounding MYOD$^+$ cells of the hypoglossal cord (Fig. 6I-J″), in a similar distribution to cells of the *Mef2c-AHF-Cre* genetic lineage (Fig. 5E,E′). These findings strongly reinforce the conclusion, based on analysis of the *Mef2c-AHF-Cre* genetic lineage, that these pharyngeal skeletal and CT elements are CPM derivatives. However, in contrast to findings with the *Mef2c-AHF-Cre* lineage, we observed *Tbx1-Cre* activated GFP$^+$ cells in muscle fibers as well as in MCT of somite-derived infrahyoid muscles (Fig. 6H). Previous evidence has suggested that *Tbx1* is activated in hypoglossal cord-derived muscles, including tongue and infrahyoid muscles, at fetal stages, after muscle patterning and differentiation (Okano et al., 2008). In support of late activation of *Tbx1* in these muscles, TBX1 is not expressed in MYOD$^+$ myogenic progenitor cells in the hypoglossal cord at E10.5 (Fig. 6I-J″).

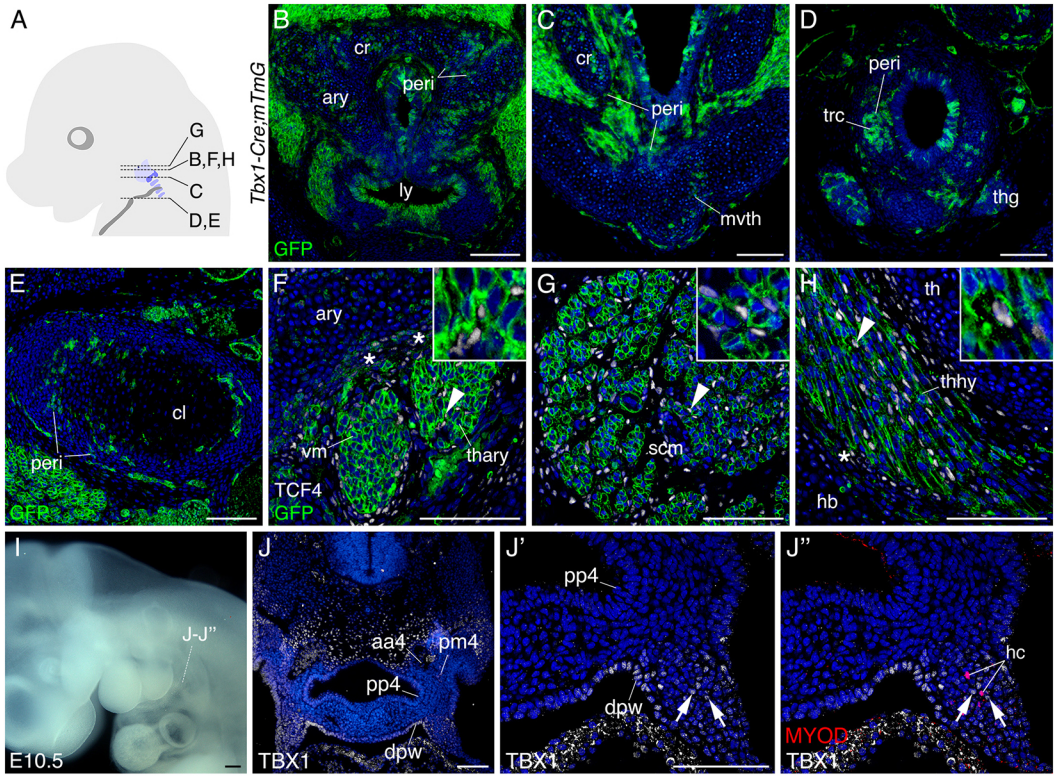

Fig. 6. *Tbx1-Cre* lineage contribution to pharyngeal and shoulder skeletons and musculoskeletal CT. (A) Diagram showing the section level of panels B to H. (B-H) GFP (B-E) and GFP and TCF4 (F-H) immunostaining of *Tbx1-Cre;mTmG* at E15.5 (*n*=5). Co-localization of GFP/TCF4 (arrowheads, magnified in insets) and the muscle attachment sites (asterisks) are indicated. *Tbx1-Cre* derivatives were detected in pharyngeal and shoulder skeletons, perichondrium, and pharyngeal and infrahyoid muscle CTs. (I) E10.5 embryo showing the section level of panels J to J″. (J-J″) TBX1 (J,J′) and TBX1/MYOD (J″) immunostaining at the 4th arch level (*n*=3). (J′,J″) High magnification of panel J showing hypoglossal cord (MYOD$^+$ TBX1$^-$) cells associated with TBX1-expressing cells (arrows). aa4, 4th pharyngeal arch artery; ary, arytenoid cartilage; cl, clavicle; cr, cricoid cartilage; dpw, dorsal pericardial wall; hb, hyoid bone; hc, hypoglossal cord; ly, laryngeal endoderm; mvth, mid-ventral part of thyroid cartilage; peri, perichondrium; pm4, 4th pharyngeal arch mesoderm; pp4, 4th pharyngeal pouch; scm, sternocleidomastoid muscle; th, thyroid cartilage; thary, thyroarytenoid muscle; thg, thyroid gland; thhy, thyrohyoid muscle; trc, tracheal cartilage; vm, vocal muscle. Scale bars: 100 µm.

Development (2020) 147, dev185256. doi:10.1242/dev.185256

Muscles with CPM-derived CT are mispatterned in *Tbx1* heterozygous mutant embryos

Haploinsufficiency for *TBX1* contributes to 22q11.2DS phenotypes in humans and *Tbx1* heterozygous mutant mice display stochastic arch artery anomalies (Scambler, 2010). With the exception of hypoplasia of the levator veli palatini, the branchiomeric myogenic program is normally activated in *Tbx1*$^{+/-}$ mice (Kelly et al., 2004; Fuchs et al., 2015). Given the contribution of *Mef2c-AHF-Cre*- and *Tbx1-Cre*-labeled CPM to CT in the pharyngeal and neck regions, we investigated skeletal muscle patterning in *Tbx1* heterozygous mutant embryos. Comparative analysis of wild-type and heterozygous mutant mice at E15.5 revealed a high frequency of patterning defects in two neck muscles in *Tbx1*$^{+/-}$ embryos (Fig. 7, Table S1). The sternocleidomastoid muscle is a branchiomeric muscle derived from the posterior PAs that normally attaches to the mastoid process and extends ventrally to the clavicle and sternum of the shoulder girdle. In *Tbx1*$^{+/-}$ embryos, however, the medial part of sternocleidomastoid muscles extended medially and connected ectopically to the greater horn of the hyoid bone (Fig. 7A-C,J,K). Such connections, observed in 8/16 *Tbx1*$^{+/-}$ embryos, were not seen in seven wild-type embryos. Similarly, the omohyoid muscle is a somite-derived infrahyoid muscle that attaches to the body of the hyoid bone and extends to the medial side of the scapula in wild-type embryos. *Tbx1*$^{+/-}$ embryos displayed ectopic connections of the omohyoid muscles to the greater horn of the hyoid bone that were not observed in wild-type embryos (Fig. 7D-F,J,K). Moreover, in *Tbx1*$^{+/-}$ embryos, the omohyoid muscle failed to extend to the normal attachment site on the scapula and instead extended abnormally to the clavicle (Fig. 7G-I,J,K). Ectopic insertions of the sternocleidomastoid and omohyoid muscles were observed both unilaterally and bilaterally, and although ectopic connections of these muscles were not correlated, the two ectopic muscles occasionally fused together when present on the same side (Fig. 7A-F, Table S1). Similarly, stochastic right and left PA artery defects are characteristic of *Tbx1*$^{+/-}$ embryos; however, no correlation was observed between lateralized muscle patterning defects and arch artery anomalies (Table S1).

Detailed investigation of *Tbx1-Cre;mTmG* embryos at E15.5 confirmed that both the sternocleidomastoid and omohyoid muscles contain MCT derived from *Tbx1*-expressing CPM (Fig. 8). Furthermore, as the *Tbx1-Cre* allele is a heterozygous null allele, we observed ectopic connections of these two muscles to the greater horn of the hyoid bone, similar to those seen in *Tbx1*$^{+/-}$ embryos (Table S1). Immunofluorescence revealed that GFP and TCF4 co-localize in the MCT of these ectopic muscles (Fig. 8D,E). As mentioned above, GFP expression was also observed in muscle

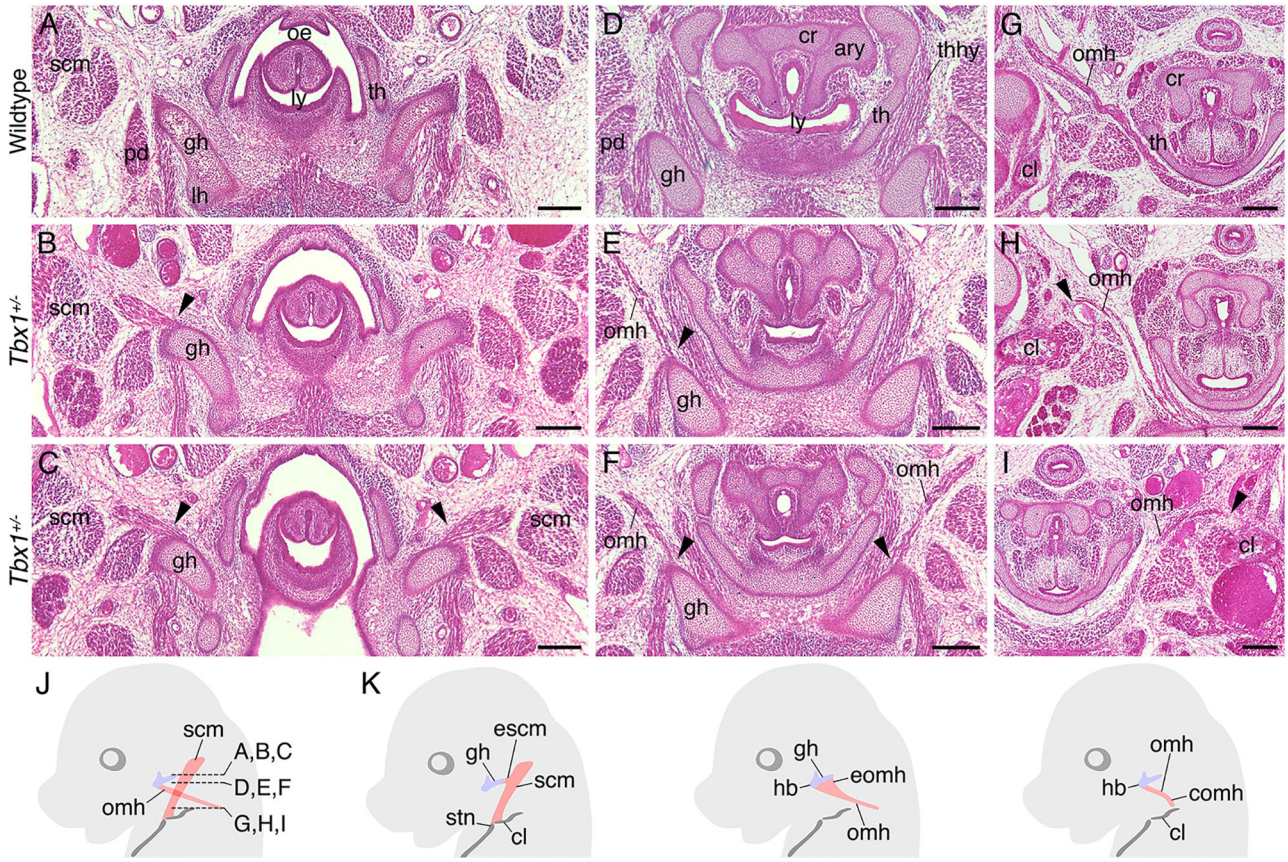

Fig. 7. Muscle patterning defects in *Tbx1* heterozygous mutant mice. (A-I) H&E sections of wild-type (*n*=7) (A,D,G) and *Tbx1*$^{+/-}$ (B,C,E,F,H,I) mice at E15.5 (*n*=16). Sternocleidomastoid and omohyoid muscles exhibit unilateral (B,E) or bilateral (C,F) ectopic connections to the greater horn of hyoid bone in *Tbx1*$^{+/-}$ mice (arrowheads). Omohyoid muscles of *Tbx1*$^{+/-}$ mice also show an abnormal extension to the clavicle (H,I, arrowheads). (J,K) Diagrams showing the transverse section levels of panels A-I and muscle patterns in wild-type (J) and *Tbx1* heterozygous mutant (K) embryos. ary, arytenoid cartilage; cl, clavicle; cr, cricoid cartilage; comh, abnormal extension of omohyoid muscle to clavicle; eomh, ectopic connection of omohyoid muscle; escm, ectopic connection of sternocleidomastoid muscle; gh, greater horn of hyoid bone; hb, hyoid bone; lh, lesser horn of hyoid bone; ly, laryngeal endoderm; oe, oesophagus; omh, omohyoid muscle; pd, posterior digastric muscle; scm, sternocleidomastoid muscle; stn, sternum manubrium; th, thyroid cartilage; thhy, thyrohyoid muscle. Scale bars: 200 µm.

Development (2020) 147, dev185256. doi:10.1242/dev.185256

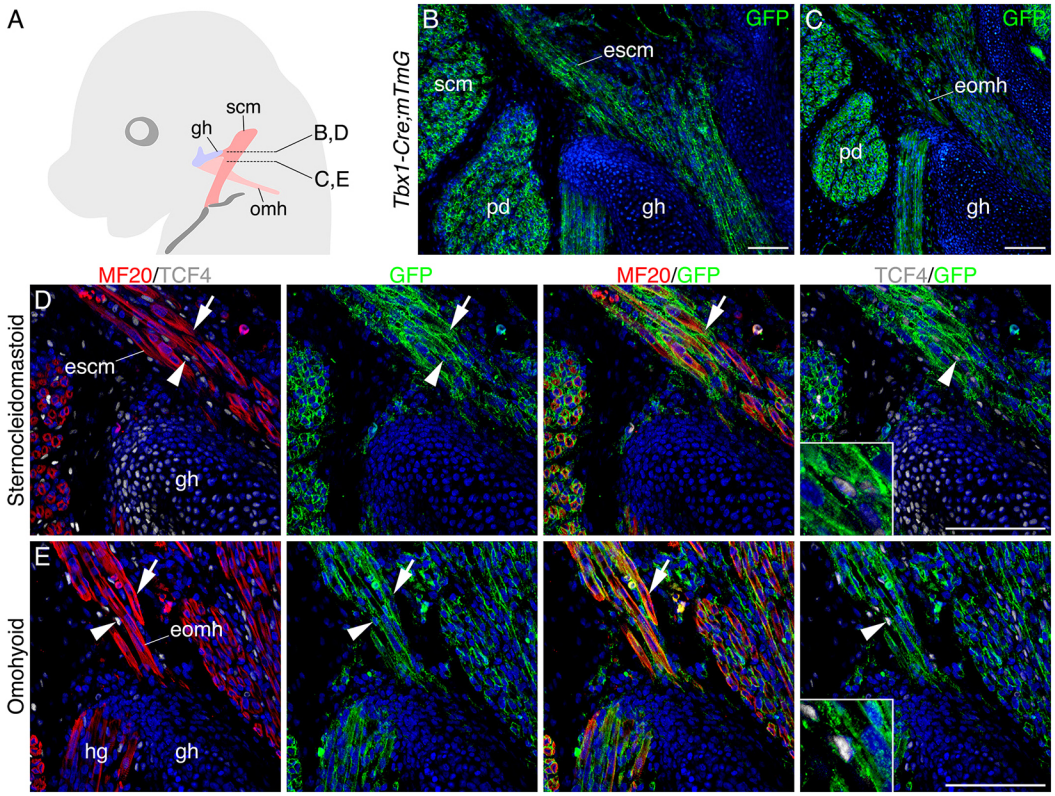

Fig. 8. *Tbx1-Cre*-derived CT in mispatterned muscles. (A) Diagram showing the transverse section levels of panels B to E. (B,C) GFP-immunostained sections from *Tbx1-Cre;mTmG* at E15.5 (*n*=5). (D,E) MF20, TCF4 and GFP immunostaining of ectopic sternocleidomastoid and omohyoid muscles. Co-localization of GFP/TCF4 (arrowheads, magnified in insets) and GFP/MF20 (arrows) are indicated. Note that *Tbx1-Cre* derivatives are detected in CT of ectopic muscles. eomh, ectopic connection of omohyoid muscle; escm, ectopic connection of sternocleidomastoid muscle; gh, greater horn of hyoid bone; hg, hyoglossus muscle; omh, omohyoid muscle; pd, posterior digastric muscle; scm, sternocleidomastoid muscle. Scale bars: 100 µm.

fibers of the infrahyoid and tongue muscles owing to the activation of *Tbx1* during the fetal period (Fig. 6H, Fig. 8). Although a late role for *Tbx1* in patterning these muscles cannot be ruled out, the arrangement of tongue muscles, characterized by NCC-derived CT, in *Tbx1* heterozygous embryos was comparable with that in wild-type embryos (Fig. 8, Fig. S7A-E). These results suggest that, subsequent to normal myogenic differentiation, biallelic expression of *Tbx1* in CPM-derived MCT is required for correct neck muscle patterning. Moreover, in $Tbx1^{-/-}$ embryos, infrahyoid muscles were formed, but severely mispatterned, displaying ectopic insertion sites on the lateral part of the clavicle and coalescence of muscle bundles; in contrast, tongue muscle pattern was normal in $Tbx1^{-/-}$ embryos (Fig. S7). Together, our results reveal that *Tbx1* is required for the correct patterning of neck muscles and provide the first evidence implicating CPM-derived CT in muscle patterning.

Neck muscle patterning defects in conditional *Tbx1* heterozygous mutant embryos

To further understand the developmental role of *Tbx1* in the CT lineage, we crossed *Mef2c-AHF-Cre* and $Tbx1^{flox/flox}$ transgenic lines (Xu et al., 2004) and observed the phenotype of *Mef2c-AHF-Cre;* $Tbx1^{flox/+}$ embryos, in which *Tbx1* is heterozygous in the *Mef2c-AHF-Cre* genetic lineage. In control $Tbx1^{flox/+}$ embryos, sternocleidomastoid and omohyoid muscles showed the normal pattern of wild-type embryos (Fig. 9A). In contrast, the omohyoid muscle in *Mef2c-AHF-Cre;* $Tbx1^{flox/+}$ embryos exhibited an ectopic connection to the greater horn of hyoid bone and an abnormal extension to the clavicle (*n*=5/7), phenotypes seen in *Tbx1* heterozygous embryos (Fig. 9B, Table S1). No patterning defects were observed in the sternocleidomastoid muscle in *Mef2c-AHF-Cre;* $Tbx1^{flox/+}$ embryos. The different penetrance of the phenotypes between *Mef2c-AHF-Cre;* $Tbx1^{flox/+}$ and $Tbx1^{+/-}$ embryos may reflect the delayed excision timing of *Tbx1* gene in the *Mef2c-AHF-Cre* genetic lineage and the relative incidence of sternocleidomastoid versus omohyoid patterning defects in $Tbx1^{+/-}$ embryos (Table S1). Together, our conditional mutant analysis demonstrates that biallelic expression of *Tbx1* in CPM-derived CT is required for normal neck muscle patterning.

DISCUSSION

The pharynx is a crucial organ for the control of food intake, swallowing, respiration and vocalization. However, despite the functional importance of the pharynx, its developmental origins remain controversial. CPM gives rise to branchiomeric skeletal muscles of the head and neck as well as SHF-derived myocardium. Here, using genetic lineage analyses we have shown that CPM has a broader developmental potential than previously recognized and contributes to a spectrum of pharyngeal structures in mice (Fig. 10, Table S2). These include cartilaginous and perichondrial cells in the medial pharyngeal and shoulder skeletons as well as MCT of pharyngeal and somite-derived infrahyoid muscles. Moreover, biallelic expression of the CPM regulatory gene *Tbx1* is required to correctly pattern neck muscles with CPM-derived MCT. Together, our results highlight the CPM origins of the mammalian pharynx, and provide new insights into the development, pathology and evolution of the pharyngeal apparatus.

Development (2020) 147, dev185256. doi:10.1242/dev.185256

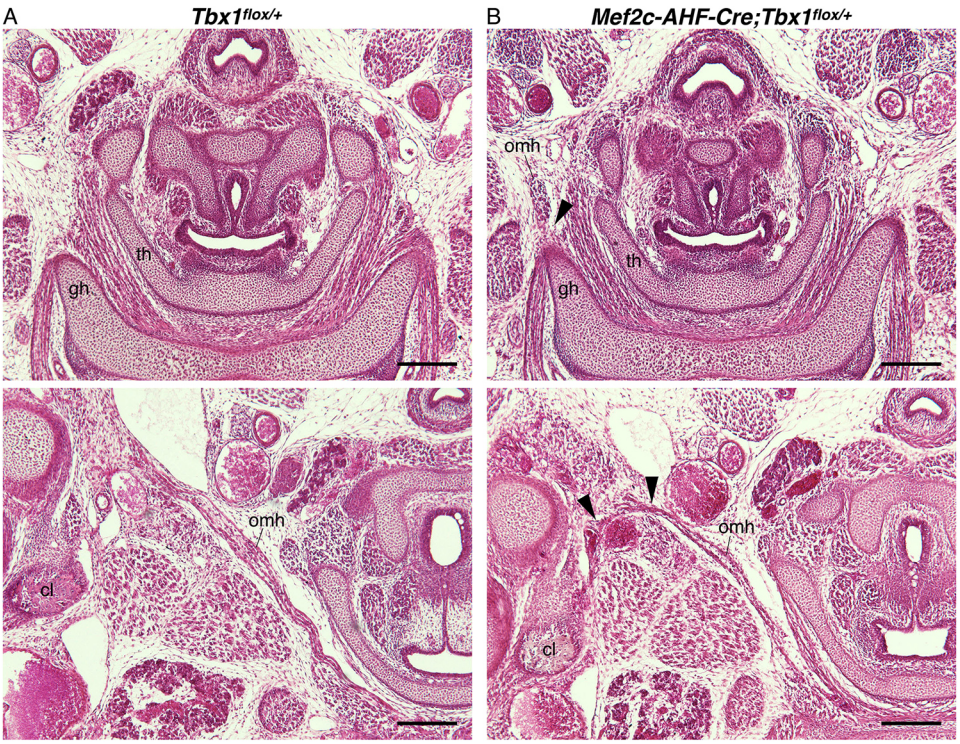

Fig. 9. Muscle patterning defects in CPM conditional *Tbx1* heterozygous mutant mice. (A,B) H&E sections of *Tbx1*$^{flox/+}$ (*n*=5) (A) and *Mef2c-AHF-Cre;Tbx1*$^{flox/+}$ (*n*=7) (B) E15.5 embryos. Omohyoid muscles show an ectopic connection to the greater horn of the hyoid bone and an abnormal extension to the clavicle (arrowheads) in *Mef2c-AHF-Cre; Tbx1*$^{flox/+}$ embryos (*n*=5 out of 7). cl, clavicle; gh, greater horn of hyoid bone; omh, omohyoid muscle; th, thyroid cartilage. Scale bars: 200 µm.

CPM origins of connective tissues and implications for muscle patterning

CPM and NCCs contribute in a complementary mediolateral pattern to the skeletons, mesenchyme and MCT of the pharynx. CPM derivatives in the pharyngeal region extend to posterior pharyngeal muscles and MCTs of branchiomeric and infrahyoid muscles, including muscle attachment sites to pharyngeal skeletons. How and when different cell fate choices are made within CPM remains to be defined. However, the contribution of CPM to MCT appears to be established early in the embryonic pharynx, where CPM is closely associated with CPM- and somite-derived muscle progenitor cells. This spatiotemporal distribution of CPM in the pharynx is similar to that of NCC-derived MCT in craniofacial structures that surround branchiomeric muscle progenitor cells and instruct muscle patterning during development (Schneider and Helms, 2003; Le Douarin et al., 2004; Noden and Trainor, 2005; Rinon et al., 2007;

A

	Skeletons/muscles	Connective tissue
Pharyngeal skeleton		
Lateral skeletons	NCCs	NCCs
Medial skeletons	CPM*	CPM
Branchiomeric muscle		
Jaw/facial muscle	CPM	NCCs
Laryngeal muscle	CPM	CPM*
Somitic muscle		
Tongue muscle	Somite	NCCs
Infrahyoid muscle	Somite	CPM*

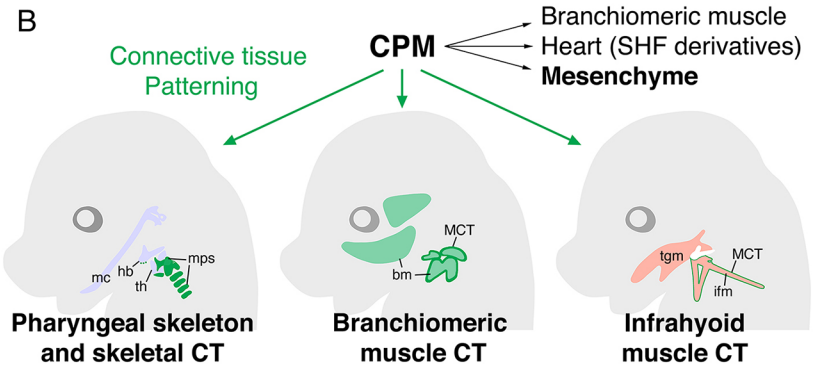

Fig. 10. Broad contribution of CPM to the mammalian pharynx. (A) Cellular origins of the mammalian pharynx. Asterisks indicate skeletons and MCT with a minor contribution from NCCs. (B) CPM contribution to different cell lineages of the mammalian pharynx. CPM-derived skeletons/connective tissue (green) and branchiomeric muscles (light green), NCC derivatives (light blue) and somitic muscles (light red) are indicated. Results from this study are indicated in bold. bm, branchiomeric muscles; CPM, cardiopharyngeal mesoderm; CT, connective tissue; hb, hyoid bone; ifm, infrahyoid muscles; mc, Meckel's cartilage; MCT, muscle connective tissue; mps, medial pharyngeal skeletons; NCCs, neural crest cells; SHF, second heart field; tgm, tongue muscles; th, thyroid cartilage.

Development (2020) 147, dev185256. doi:10.1242/dev.185256

Grenier et al., 2009; Tokita and Schneider, 2009; Gitton et al., 2010). Our results thus raise the hypothesis that CPM, like NCCs, may confer patterning information on muscles during morphogenesis of the mammalian pharynx. For example, the differential origins of MCT within individual muscles may contribute to ensuring correct attachment to mesodermal and NCC-derived musculoskeletal elements (Heude et al., 2018). Moreover, as NCC derivatives are implicated in the formation of innervation pattern in craniofacial elements (Köntges and Lumsden, 1996; Begbie and Graham, 2001), the relative contribution of CPM and NCCs to MCT may be linked to muscle innervation in the pharynx. Indeed, muscles innervated by the recurrent branch of the vagus nerve have mostly CPM-derived MCT, whereas the cricothyroid muscle, innervated by the superior laryngeal branch of the vagus nerve, has extensive NCC MCT contributions. Similarly, infrahyoid muscles with extensive CPM-derived MCT have cervical innervation (ansa cervicalis), whereas the thyrohyoid muscle with predominantly NCC-derived MCT is innervated by a branch of the hypoglossal nerve. These observations point to similar developmental roles of CPM and NCC in muscle patterning and innervation.

The T-box transcription factor *Tbx1* is a crucial regulator of CPM and pharyngeal development. In support of a CPM origin of infrahyoid MCT, TBX1 is expressed in cells surrounding the hypoglossal cord at midgestation, in a similar distribution to *Mef2c-AHF-Cre* derivatives. At fetal stages, *Tbx1-Cre;mTmG* labels infrahyoid muscle myofibers as well as MCT, consistent with later activation of *Tbx1* in the myogenic lineage. We found that heterozygous *Tbx1* mutant embryos exhibit defective patterning of both branchiomeric and somite-derived neck muscles containing CT derived from *Mef2c-AHF-Cre* and *Tbx1-Cre* genetic lineages. In particular, the sternocleidomastoid and omohyoid muscles ectopically connect to the greater horn of the hyoid bone in $Tbx1^{+/-}$ embryos. Moreover, homozygous *Tbx1* mutant embryos show a patterning defect in infrahyoid muscles, with ectopic insertion into the clavicle. Although we cannot exclude that later *Tbx1* expression in the muscle lineage contributes to the observed patterning defects, tongue muscles with MCT exclusively derived from NCC are patterned normally in *Tbx1* mutants, despite also upregulating *Tbx1* expression after differentiation (Okano et al., 2008). Moreover, with the exception of the 4th arch-derived levator veli palatini, which is hypoplastic but correctly patterned, branchiomeric muscles in *Tbx1* heterozygous mutants, and even hypoplastic first arch-derived muscles in *Tbx1* null embryos, are patterned normally (Kelly et al., 2004; Grifone et al., 2008; Fuchs et al., 2015). Crucially, conditional mutant mice with the deletion of one *Tbx1* allele in the *Mef2c-AHF-Cre* lineage display similar muscle patterning defects to those seen in $Tbx1^{+/-}$ mice. As the *Mef2c-AHF-Cre* lineage contributes to MCT but not to myofibers of the omohyoid muscle, this result strongly supports a role for CPM-derived MCT in neck muscle patterning. Together, our data demonstrate that biallelic *Tbx1* is required for patterning of a subset of neck muscles and implicate CPM in muscle patterning during pharyngeal development.

We note that several muscles with CPM MCTs retain the normal pattern in heterozygous and conditional heterozygous mutants of *Tbx1*, possibly because of differential dependency on *Tbx1* in different muscles. *Tbx1* is downregulated early in medial posterior mesoderm of the embryonic pharynx (De Bono et al., 2018), and other genes may play a patterning role for the medial pharyngeal components such as intrinsic laryngeal muscles. Alternatively, as some muscles have MCT from the NCC lineage, NCC-derived MCT may compensate for impaired CPM-derived MCT in mutant embryos. Although a previous study reported a hyoid bone defect on conditional null mutation of *Tbx1* in *Wnt1-Cre* derivatives, no muscular phenotypes were noted (Funato et al., 2015). Further analyses of lineage-specific *Tbx1* mutants, as well as comparison of the gene regulatory networks operating in CPM and NCC-derived CT, will be required to elucidate the cellular basis of the patterning defect. Interestingly, although *Mef2c-AHF-Cre* is exclusively expressed in CPM, other enhancers from the *Mef2c* locus have been shown to drive expression in NCCs (Aoto et al., 2015; Hu et al., 2015).

Muscle patterning defects and insights into 22q11.2 deletion syndrome

Our identification of muscular patterning defects in the pharynx of *Tbx1* heterozygous mutants extends the known haploinsufficient phenotypes in this mouse model. The majority of 22q11.2DS patients, haploinsufficient for a multigene deletion including *TBX1*, show velopharyngeal insufficiency, facial asymmetry, and feeding and speech problems (Rommel et al., 1999; Eicher et al., 2000; Dyce et al., 2002; McDonald-McGinn et al., 2015). A study further showed that 22q11.2DS patients frequently suffer from dysphagia and feeding difficulties, independent from palatal and cardiac anomalies, and that pharyngeal opening by movement of the hyoid bone is impaired for unknown reasons (Eicher et al., 2000). Given the importance of the hyoid bone for proper function of the pharyngeal apparatus (McFarland, 2009), the patterning defects observed in the sternocleidomastoid and omohyoid muscles of *Tbx1* heterozygous mutant mice suggest a potential explanation for pharyngeal dysfunction in 22q11.2DS patients. Indeed, ectopic connections of these muscles to the greater horn of hyoid bone is likely to affect the mobility of the bone. Further characterization of these muscle patterning defects will provide mechanistic insights into the underlying pathology. Moreover, if similar defects underlie feeding and speech difficulties in 22q11.2DS patients, they could be targets for surgical intervention.

CPM and NCC rearrangement during evolution of the vertebrate pharynx

The pharynx has undergone various morphological changes in vertebrate history (Romer and Parsons, 1977). Remarkable is the remodeling of gills and the gain of laryngopharyngeal skeletons in the tetrapod lineage as it adopted a terrestrial lifestyle (Coates et al., 2008). As it has been long assumed that skeletons in the tetrapod pharynx are homologous with gill skeletons in fishes (Gegenbaur, 1892; Goodrich, 1930; Romer and Parsons, 1977), the embryonic source of those skeletons, NCCs, have been the major subject of analysis. Many studies have demonstrated the contribution of NCCs to the pharyngeal apparatus in different vertebrate taxa (Schilling and Kimmel, 1994; Köntges and Lumsden, 1996; Olsson and Hanken, 1996; Le Douarin et al., 2004; Matsuoka et al., 2005; Noden and Trainor, 2005; Martin et al., 2009; Kague et al., 2012; Mongera et al., 2013). Among the pharyngeal structures we identify as having CPM origins, such as medial pharyngeal cartilages and MCTs, some have been previously thought to derive from NCCs or LPM (Noden, 1988; Matsuoka et al., 2005). However, genetic lineage tracing using *Wnt1-Cre* shows a minimal contribution of NCCs to medial pharyngeal cartilages and MCTs (Fig. 1, Fig. S5; Tabler et al., 2017; Heude et al., 2018). In contrast, a mesodermal contribution to the medial pharyngeal skeleton has been suggested in avians and recently shown using *Mesp1-Cre* lineage tracing in the mouse (Noden, 1988; Tabler et al., 2017). Consistent with

Development (2020) 147, dev185256. doi:10.1242/dev.185256

heterogeneous origins of pharyngeal skeletal elements, several studies have noted distinct outcomes in the posterior pharyngeal skeleton after genetic perturbations (see discussion in Tabler et al., 2017). However, *Mesp1* is expressed in cranial and anterior somitic mesoderm as well as LPM; our results using two different *Cre* lines now identify CPM as the source of medial skeletons, CT and mesenchymal cells in the mammalian pharynx.

Our comparison of *Mef2c-AHF-Cre* and *Wnt1-Cre* genetic lineage contributions shows that NCCs give rise to lateral skeletal elements, CTs and mesenchyme in the pharynx, in a complementary distribution to medially localized CPM derivatives. These findings are consistent with lineage analyses in axolotl, showing that NCCs contribute to the lateral visceral skeletons, whereas the second basibranchial skeleton, the mid-ventral element of the pharynx, originates from the mesoderm associated with pharyngeal muscles and outflow tract (Davidian and Malashichev, 2013; Sefton et al., 2015). Furthermore, based on histological observations in frogs and salamanders, Edgeworth (1935) proposed that mesodermal cells contiguous with the dorsal pericardial wall spread medially around the posterior pharyngeal endoderm to form arytenoid, cricoid and tracheal cartilages, consistent with our genetic evidence that CPM and NCC derivatives distribute in a mediolateral complementary pattern in the pharynx and posterior PA of mouse embryos. The cellular distribution at this level is unique and not found in anterior PAs in mice, nor in fish PAs, suggesting that it is a synapomorphy of the tetrapod lineage (Fig. S8A) (McCauley and Bronner-Fraser, 2006; Abrial et al., 2017; Adachi et al., 2018). Our finding that arch 6 develops differently to anterior arches is consistent with a recent study by Poopalasundaram et al. (2019) showing that posterior PA development in amniotes is markedly distinct from that in other vertebrate clades. However, although Poopalasundaram et al. suggest that myogenesis is suppressed in posterior PAs, we observed MYOD protein accumulation in posterior CPM in the anlagen of branchiomeric muscles derived from arches 4-6 from early developmental stages. The unique cellular distribution of CPM and NCCs in the posterior PA region has important implications for the evolution of the vertebrate pharynx. CPM-derived medial pharyngeal skeletons likely represent evolutionary novelties in the tetrapod lineage, whereas the hyoid bone and lateral thyroid cartilage in mammals are comparable with NCC-derived pharyngeal skeletons in non-tetrapod vertebrates (Fig. S8A,B). Moreover, rearrangement of the distribution of mesenchymal cell populations in the posterior PAs may have contributed to the morphological transition of pharyngeal skeletons during early tetrapod history.

MATERIALS AND METHODS

Transgenic mice

Transgenic lines used in this study have been described previously: *Mef2c-AHF-Cre* (Verzi et al., 2005), *Wnt1-Cre* (Danielian et al., 1998), *Tbx1-Cre* (Huynh et al., 2007), *Rosa26-nlacZ* (Soriano, 1999), *Rosa26-YFP* (Srinivas et al., 2001), *Rosa26-mTmG* (Muzumdar et al., 2007), $Tbx1^{+/-}$ (Jerome and Papaioannou, 2001) and $Tbx1^{flox/flox}$ (Xu et al., 2004). Mice were maintained on a mixed background and genotyped using PCR. Noon of the day of the vaginal plug observation was defined as E0.5 and embryos were staged according to Kaufman (1992). Animal experiments were conducted in agreement with National and European laws and approved by the Ethics Committee for Animal Experimentation of Marseille and the French Ministry for National Education, Higher Education and Research.

Histological analysis

Embryos were fixed in 4% paraformaldehyde (PFA) and washed in phosphate buffered saline (PBS). Fixed embryos were embedded in paraffin (Paraplast X-TRA, P3808-1KG, Merck Sigma-Aldrich) and sectioned at 10 µm thickness. Sections were stained with hematoxylin and eosin solutions (H&E; Harris Hematoxylin, HHS32-1L and Eosin Y, HT110132-1L, Merck Sigma-Aldrich) and then imaged using an Axio Zoom.V16 microscope with an Axiocam 512 color camera (ZEISS).

Immunofluorescence

Immunofluorescence on paraffin sections was performed as described previously (De Bono et al., 2018). Antigen unmasking solution [10 mM Tris-HCl (pH 9.5), 1 mM EDTA and 0.05% Tween20] was used to reveal epitopes. The following primary and secondary antibodies were used: chicken anti-GFP (1/500, ab13970, Abcam and 1/500, GFP-1020, Aves), mouse anti-MHC1 (1/50, MF20, Developmental Studies Hybridoma Bank), rabbit anti-TBX1 (1/100, Ls-C31179, LSBio), rabbit anti-TCF4 (1/150, C48H11, Cell Signaling Technology), rat anti-MYOD (1/200, 39991, Active Motif), Alexa donkey anti-chicken 488, Alexa donkey anti-mouse 568 and Alexa donkey anti-rabbit 647 (1/500, Thermo Fisher Scientific). The TSA Plus system was employed to detect MYOD (NEL741001KT, PerkinElmer). For paraffin sections of *Wnt1-Cre;RYFP* and *Mef2c-AHF-Cre;RYFP* at E10.5, embryos were first incubated in low melting point paraffin and then mounted in paraffin (Avé et al., 1997) (1071501000, Merck Millipore). Immunostained sections were counterstained with Hoechst 33258 (1/1000, 861405, Merck Sigma-Aldrich) and imaged using an Axio Zoom.V16 microscope with an Axiocam 512 color camera and Axio Imager APO Z1 (ZEISS).

Section *in situ* hybridization

The method of *in situ* hybridization on paraffin sections has been described previously (De Bono et al., 2018). *Cre* expressions of sections at pharyngeal, shoulder and heart levels were tested on the same microscope slide. The hybridization was performed at 70°C (n=4), 65°C (n=3) and 60°C (n=3). For signal detection, anti-Digoxigenin-AP antibodies (1/2000, 11093274910, Roche) and BM purple (11442074001, Roche) were used, and after color development, sections were counterstained with eosin and imaged using Axio Zoom.V16 with Axiocam 512 color camera (ZEISS).

X-gal staining

Embryos were fixed in 4% PFA for 20 min at 4°C and stained in X-gal staining solution (0.1% X-gal, 2 mM $MgCl_2$, 0.01% deoxycholate, 0.02% Nonidet P40, 5 mM potassium ferricyanide, 5 mM potassium ferrocyanide and PBS) for 2-3 h at 37°C. Embryos were then re-fixed in 4% PFA, washed in PBS, and imaged using Axio Zoom.V16 with Axiocam 512 color camera (ZEISS).

Acknowledgements

We are grateful to Kelly team members and E. Heude, F. Sugahara, G. Comai, J. Lemberg, J. Yamaguchi, S. Kuroda, W. Takagi and P. Janvier for discussions, and to A. Grimaldi, F. Helmbacher and S. Tajbakhsh for critical reading of the manuscript.

Competing interests

The authors declare no competing or financial interests.

Author contributions

Conceptualization: N.A., R.G.K.; Methodology: N.A., R.G.K.; Validation: N.A.; Investigation: N.A.; Resources: N.A., M.B., A.B., R.G.K.; Data curation: N.A., R.G.K.; Writing - original draft: N.A.; Writing - review & editing: N.A., A.B., R.G.K.; Visualization: N.A., R.G.K.; Supervision: R.G.K.; Project administration: N.A., R.G.K.; Funding acquisition: N.A., R.G.K.

Funding

This study received support from Bourses du Gouvernement Français (to N.A.), Yamada Science Foundation (2017-5013, to N.A.), Fondation pour la Recherche Médicale (DEQ20150331717, to R.G.K.), AFM-Téléthon (to R.G.K.), Agence Nationale de la Recherche (Heartbox project to R.G.K.) and Fondation Leducq (Transatlantic Network of Excellence 15CVD01, to R.G.K. and A.B.).

Supplementary information

Supplementary information available online at
http://dev.biologists.org/lookup/doi/10.1242/dev.185256.supplemental

Peer review history

The peer review history is available online at https://dev.biologists.org/lookup/doi/10.1242/dev.185256.reviewer-comments.pdf

References

Abrial, M., Paffett-Lugassy, N., Jeffrey, S., Jordan, D., O'Loughlin, E., Frederick, C. J., III, Burns, C. G. and Burns, C. E. (2017). TGF-β Signaling is necessary and sufficient for pharyngeal arch artery angioblast formation. *Cell Rep.* **20**, 973-983. doi:10.1016/j.celrep.2017.07.002

Adachi, N., Pascual-Anaya, J., Hirai, T., Higuchi, S. and Kuratani, S. (2018). Development of hypobranchial muscles with special reference to the evolution of the vertebrate neck. *Zool. Lett.* **4**, 1-13. doi:10.1186/s40851-018-0087-x

Aoto, K., Sandell, L. L., Butler Tjaden, N. E., Yuen, K. C., Watt, K. E. N., Black, B. L., Durnin, M. and Trainor, P. A. (2015). Mef2c-F10N enhancer driven β-galactosidase (LacZ) and Cre recombinase mice facilitate analyses of gene function and lineage fate in neural crest cells. *Dev. Biol.* **402**, 3-16. doi:10.1016/j.ydbio.2015.02.022

Avé, P., Colucci-Guyon, E., Babinet, C. and Huerre, M. R. (1997). An improved method to detect β-galactosidase activity in transgenic mice: a post-staining procedure on paraffin embedded tissue sections. *Transgenic Res.* **6**, 37-40. doi:10.1023/A:1018401015497

Begbie, J. and Graham, A. (2001). Integration between the epibranchial placodes and the hindbrain. *Science* **294**, 595-598. doi:10.1126/science.1062028

Beverdam, A., Merlo, G. R., Paleari, L., Mantero, S., Genova, F., Barbieri, O., Janvier, P. and Levi, G. (2002). Jaw Transformation with gain of symmetry after Dlx5/Dlx6 inactivation: mirror of the past? *Genesis* **34**, 221-227. doi:10.1002/gene.10156

Buckingham, M. and Vincent, D. (2009). Distinct and dynamic myogenic populations in the vertebrate embryo. *Curr. Opin. Genet. Dev.* **19**, 444-453. doi:10.1016/j.gde.2009.08.001

Cai, C. L., Liang, X., Shi, Y., Chu, P. H., Pfaff, S. L., Chen, J. and Evans, S. (2003). Isl1 identifies a cardiac progenitor population that proliferates prior to differentiation and contributes a majority of cells to the heart. *Dev. Cell* **5**, 877-889. doi:10.1016/S1534-5807(03)00363-0

Chai, Y., Jiang, X., Ito, Y., Bringas, P., Jr., Han, J., Rowitch, D. H., Soriano, P., McMahon, A. P. and Sucov, H. M. (2000). Fate of the mammalian cranial neural crest during tooth and mandibular morphogenesis. *Development* **127**, 1671-1679.

Coates, M. I., Ruta, M. and Friedman, M. (2008). Ever since owen: changing perspectives on the early evolution of tetrapods. *Annu. Rev. Ecol. Evol. Syst.* **39**, 571-592. doi:10.1146/annurev.ecolsys.38.091206.095546

Danielian, P. S., Muccino, D., Rowitch, D. H., Michael, S. K. and McMahon, A. P. (1998). Modification of gene activity in mouse embryos in utero by a tamoxifen-inducible form of Cre recombinase. *Curr. Biol.* **8**, 1323-13S2. doi:10.1016/S0960-9822(07)00562-3

Dastjerdi, A., Robson, L., Walker, R., Hadley, J., Zhang, Z., Rodriguez-niedenfu, M., Ataliotis, P., Baldini, A., Scambler, P. and Francis-west, P. (2007). Tbx1 regulation of myogenic differentiation in the limb and cranial mesoderm. *Dev. Dyn.* **236**, 353-363. doi:10.1002/dvdy.21010

Davidian, A. and Malashichev, Y. (2013). Dual embryonic origin of the hyobranchial apparatus in the Mexican axolotl (Ambystoma mexicanum). *Int. J. Dev. Biol.* **57**, 821-828. doi:10.1387/ijdb.130213ym

De Bono, C., Thellier, C., Bertrand, N., Sturny, R., Jullian, E., Cortes, C., Stefanovic, S., Zaffran, S., Théveniau-Ruissy, M. and Kelly, R. G. (2018). T-box genes and retinoic acid signaling regulate the segregation of arterial and venous pole progenitor cells in the murine second heart field. *Hum. Mol. Genet.* **27**, 3747-3760. doi:10.1093/hmg/ddy266

Depew, M. J., Lufkin, T. and Rubenstein, J. L. (2002). Specification of jaw subdivisions by Dlx genes. *Science*. **298**, 381-385. doi:10.1126/science.1075703

Diogo, R., Kelly, R. G., Christiaen, L., Levine, M., Ziermann, J. M., Molnar, J. L., Noden, D. M. and Tzahor, E. (2015). A new heart for a new head in vertebrate cardiopharyngeal evolution. *Nature* **520**, 466-473. doi:10.1038/nature14435

Dyce, O., Mcdonald-mcginn, D., Kirschner, R. E., Zackai, E., Young, K. and Jacobs, I. N. (2002). Otolaryngologic Manifestations of the 22q11.2 Deletion Syndrome. *Arch. Otolaryngol. Head Neck Surg.* **128**, 1408-1412. doi:10.1001/archotol.128.12.1408

Edgeworth, F. (1935). *The Cranial Muscles of Vertebrates*. Cambridge at the University Press.

Eicher, P. S., McDonald-McGinn, D. M., Fox, C. A., Driscoll, D. A., Emanuel, B. S. and Zackai, E. H. (2000). Dysphagia in children with a 22q11.2 deletion: Unusual pattern found on modified barium swallow. *J. Pediatr.* **137**, 158-164. doi:10.1067/mpd.2000.105356

Foster, K., Sheridan, J., Veiga-Fernandes, H., Roderick, K., Pachnis, V., Adams, R., Blackburn, C., Kioussis, D. and Coles, M. (2008). Contribution of neural crest-derived cells in the embryonic and adult thymus. *J. Immunol.* **180**, 3183-3189. doi:10.4049/jimmunol.180.5.3183

Fuchs, J. C., Linden, J. F., Baldini, A. and Tucker, A. S. (2015). A defect in early myogenesis causes Otitis media in two mouse models of 22q11. 2 Deletion Syndrome. *Hum. Mol. Genet.* **24**, 1869-1882. doi:10.1093/hmg/ddu604

Funato, N., Nakamura, M., Richardson, J. A., Srivastava, D. and Yanagisawa, H. (2015). Loss of Tbx1 induces bone phenotypes similar to cleidocranial dysplasia. *Hum. Mol. Genet.* **24**, 424-435. doi:10.1093/hmg/ddu458

Gegenbaur, C. (1892). *Die Epiglottis, Vergleichend-Anatomische Studie*. Leipzig: Wilhelm Engelmann.

Gitton, Y., Heude, É., Vieux-rochas, M., Benouaiche, L., Fontaine, A., Sato, T., Kurihara, Y., Kurihara, H., Couly, G. and Levi, G. (2010). Evolving maps in craniofacial development. *Semin. Cell Dev. Biol.* **21**, 301-308. doi:10.1016/j.semcdb.2010.01.008

Goddeeris, M. M., Rho, S., Petiet, A., Davenport, C. L., Johnson, G. A., Meyers, E. N. and Klingensmith, J. (2008). Intracardiac septation requires hedgehog-dependent cellular contributions from outside the heart. *Development* **135**, 1887-1895. doi:10.1242/dev.016147

Goodrich, E. (1930). *Studies on the Structure and Development of Vertebrates*. London: MacMillan and Co., Limited.

Gopalakrishnan, S., Comai, G., Sambasivan, R., Francou, A., Kelly, R. G. and Tajbakhsh, S. (2015). A cranial mesoderm origin for esophagus striated muscles. *Dev. Cell* **34**, 694-704. doi:10.1016/j.devcel.2015.07.003

Grenier, J., Teillet, M.-A., Grifone, R., Kelly, R. G. and Duprez, D. (2009). Relationship between neural crest cells and cranial mesoderm during head muscle development. *PLoS ONE* **4**, e4381. doi:10.1371/journal.pone.0004381

Grifone, R., Jarry, T., Dandonneau, M., Grenier, J., Duprez, D. and Kelly, R. G. (2008). Properties of branchiomeric and somite- derived muscle development in Tbx1 mutant. *Dev. Dyn.* **237**, 3071-3078. doi:10.1002/dvdy.21718

Heude, E., Tesarova, M., Sefton, E. M., Jullian, E., Adachi, N., Grimaldi, A., Zikmund, T., Kaiser, J., Kardon, G., Kelly, R. G. et al. (2018). Unique morphogenetic signatures define mammalian neck muscles and associated connective tissues. *Elife* **7**, e40179. doi:10.7554/eLife.40179.029

Hu, J., Verzi, M. P., Robinson, A. S., Tang, P. L. F., Hua, L. L., Xu, S. M., Kwok, P. Y. and Verzi, M. P. (2015). Endothelin signaling activates Mef2c expression in the neural crest through a MEF2C-dependent positive-feedback transcriptional pathway. *Dev.* **142**, 2775-2780. doi:10.1242/dev.126391

Huang, R., Zhi, Q., Patel, K., Wilting, J. and Christ, B. (2000). Dual origin and segmental organisation of the avian scapula. *Development* **127**, 3789-3794.

Huynh, T., Chen, L., Terrell, P. and Baldini, A. (2007). A fate map of Tbx1 expressing cells reveals heterogeneity in the second cardiac field. *Genesis* **45**, 470-475. doi:10.1002/dvg.20317

Jerome, L. A. and Papaioannou, V. E. (2001). DiGeorge syndrome phenotype in mice mutant for the T-box gene, Tbx1. *Nat. Genet.* **27**, 286-291. doi:10.1038/85845

Jiang, X., Rowitch, D. H., Soriano, P., McMahon, A. P. and Sucov, H. M. (2000). Fate of the mammalian cardiac neural crest. *Development* **127**, 1607-1616.

Kague, E., Gallagher, M., Burke, S., Parsons, M., Franz-Odendaal, T. and Fisher, S. (2012). Skeletogenic fate of zebrafish cranial and trunk neural crest. *PLoS ONE* **7**, 1-13. doi:10.1371/journal.pone.0047394

Kardon, G., Harfe, B. D. and Tabin, C. J. (2003). A Tcf4-positive mesodermal population provides a prepattern for vertebrate limb muscle patterning. *Dev. Cell* **5**, 937-944. doi:10.1016/S1534-5807(03)00360-5

Kaufman, M. H. (1992). *The Atlas of Mouse Development*. Cambridge, UK: Academic.

Kelly, R. G., Brown, N. A. and Buckingham, M. E. (2001). The arterial pole of the mouse heart forms from Fgf10-expressing cells in pharyngeal mesoderm. *Dev. Cell* **1**, 435-440. doi:10.1016/S1534-5807(01)00040-5

Kelly, R. G., Jerome-Majewska, L. A. and Papaioannou, V. E. (2004). The del22q11.2 candidate gene Tbx1 regulates branchiomeric myogenesis. *Hum. Mol. Genet.* **13**, 2829-2840. doi:10.1093/hmg/ddh304

Kong, P., Racedo, S. E., Macchiarulo, S., Hu, Z., Carpenter, C., Guo, T., Wang, T., Zheng, D. and Morrow, B. E. (2014). Tbx1 is required autonomously for cell survival and fate in the pharyngeal core mesoderm to form the muscles of mastication. *Hum. Mol. Genet.* **23**, 4215-4231. doi:10.1093/hmg/ddu140

Köntges, G. and Lumsden, A. (1996). Rhombencephalic neural crest segmentation is preserved throughout craniofacial ontogeny. *Development* **3242**, 3229-3242.

Le Douarin, N. M., Creuzet, S., Couly, G. and Dupin, E. (2004). Neural crest cell plasticity and its limits. *Development* **131**, 4637-4650. doi:10.1242/dev.01350

Lescroart, F., Kelly, R. G., Le Garrec, J.-F., Nicolas, J.-F., Meilhac, S. M. and Buckingham, M. (2010). Clonal analysis reveals common lineage relationships between head muscles and second heart field derivatives in the mouse embryo. *Development* **137**, 3269-3279. doi:10.1242/dev.050674

Lescroart, F., Hamou, W., Francou, A., Théveniau-Ruissy, M., Kelly, R. G. and Buckingham, M. (2015). Clonal analysis reveals a common origin between nonsomite-derived neck muscles and heart myocardium. *Proc. Natl. Acad. Sci. USA* **112**, 1446-1451. doi:10.1073/pnas.1424538112

Lindsay, E. A., Vitelli, F., Su, H., Morishima, M., Huynh, T., Pramparo, T., Jurecic, V., Ogunrinu, G., Sutherland, H. F., Scambler, P. J. et al. (2001). Tbx1 haploinsufficiency in the DiGeorge syndrome region causes aortic arch defects in mice. *Nature* **6836**, 97-101. doi:10.1038/35065105

Mackenzie, S., Walsh, F. S. and Graham, A. (1998). Migration of hypoglossal myoblast precursors. *Dev. Dyn.* **213**, 349-358. doi:10.1002/(SICI)1097-0177(199812)213:4<349::AID-AJA1>3.0.CO;2-6

Martin, W. M., Bumm, L. A. and McCauley, D. W. (2009). Development of the viscerocranial skeleton during embryogenesis of the sea lamprey, petromyzon marinus. *Dev. Dyn.* **238**, 3126-3138. doi:10.1002/dvdy.22164

Matsuoka, T., Ahlberg, P. E., Kessaris, N., Iannarelli, R., Dennehy, U., Richardson, W. D., McMahon, A. P. and Koentges, G. (2005). Neural crest origins of the neck and shoulder. *Nature* **436**, 347-355. doi:10.1038/nature03837

McCauley, D. W. and Bronner-Fraser, M. (2006). Importance of SoxE in neural crest development and the evolution of the pharynx. *Nature* **441**, 750-752. doi:10.1038/nature04691

McDonald-mcGinn, D. M., Sullivan, K. E., Marino, B., Philip, N., Swillen, A., Vorstman, J. A. S., Zackai, E. H. and Emanuel, B. S. (2015). 22q11.2 deletion syndrome. *Nat. Rev. Dis. Prim.* **1**, 15071. doi:10.1038/nrdp.2015.71

McFarland, D. H. (2009). *Netter's Atlas of Anatomy for Speech, Swallowing, and Hearing*. Mosby/Elsevier.

Merscher, S., Funke, B., Epstein, J. A., Heyer, J., Puech, A., Lu, M. M., Xavier, R. J., Demay, M. B., Russell, R. G., Factor, S. et al. (2001). TBX1 Is responsible for cardiovascular defects in velo-cardio-facial/digeorge syndrome. *Cell* **104**, 619-629. doi:10.1016/S0092-8674(01)00247-1

Minoux, M. and Rijli, F. M. (2010). Molecular mechanisms of cranial neural crest cell migration and patterning in craniofacial development. *Development* **137**, 2605-2621. doi:10.1242/dev.040048

Minoux, M., Antonarakis, G. S., Kmita, M., Duboule, D. and Rijli, F. M. (2009). Rostral and caudal pharyngeal arches share a common neural crest ground pattern. *Development* **136**, 637-645. doi:10.1242/dev.028621

Mongera, A., Singh, A. P., Levesque, M. P., Chen, Y.-Y., Konstantinidis, P. and Nusslein-Volhard, C. (2013). Genetic lineage labeling in zebrafish uncovers novel neural crest contributions to the head, including gill pillar cells. *Development* **140**, 916-925. doi:10.1242/dev.091066

Muzumdar, M. D., Tasic, B., Miyamichi, K., Li, L. and Luo, L. (2007). A global double-fluorescent cre reporter mouse. *Genesis* **45**, 593-605. doi:10.1002/dvg.20335

Noden, D. M. (1988). Interactions and fates of avian craniofacial mesenchyme. *Development* **103**, 121-140.

Noden, D. M. and Trainor, P. A. (2005). Relations and interactions between cranial mesoderm and neural crest populations. *J. Anat.* **207**, 575-601. doi:10.1111/j.1469-7580.2005.00473.x

Okano, J., Sakai, Y. and Shiota, K. (2008). Retinoic acid down-regulates Tbx1 expression and induces abnormal differentiation of tongue muscles in fetal mice. *Dev. Dyn.* **237**, 3059-3070. doi:10.1002/dvdy.21715

Olsson, L. and Hanken, J. (1996). Cranial neural-crest migration and chondrogenic fate in the oriental fire-bellied toad bombina orientalis: defining the ancestral pattern of head development in anuran amphibians. *J. Morphol.* **229**, 105-120. doi:10.1002/(SICI)1097-4687(199607)229:1<105::AID-JMOR7>3.0.CO;2-2

Poopalasundaram, S., Richardson, J., Scott, A., Donovan, A., Liu, K. and Graham, A. (2019). Diminution of pharyngeal segmentation and the evolution of the amniotes. *Zool. Lett.* **5**, 387. doi:10.1186/s40851-019-0123-5

Rinon, A., Lazar, S., Marshall, H., Buchmann-Moller, S., Neufeld, A., Elhanany-Tamir, H., Taketo, M. M., Sommer, L., Krumlauf, R. and Tzahor, E. (2007). Cranial neural crest cells regulate head muscle patterning and differentiation during vertebrate embryogenesis. *Development* **134**, 3065-3075. doi:10.1242/dev.002501

Romer, A. S. and Parsons, T. S. (1977). *The Vertebrate Body*. Saunders.

Rommel, N., Vantrappen, G., Swillen, A., Devriendt, K., Feenstra, L. and Fryns, J. (1999). Retrospective analysis of feeding and speech disorders in 50 patients with velo-cardio-facial syndrome. *Genet. Couns.* **10**, 71-78.

Sambasivan, R., Gayraud-morel, B., Dumas, G., Cimper, C., Paisant, S., Kelly, R. G. and Tajbakhsh, S. (2009). Distinct regulatory cascades govern extraocular and pharyngeal arch muscle progenitor cell Fates. *Dev. Cell* **16**, 810-821. doi:10.1016/j.devcel.2009.05.008

Sambasivan, R., Kuratani, S. and Tajbakhsh, S. (2011). An eye on the head: the development and evolution of craniofacial muscles. *Development* **138**, 2401-2415. doi:10.1242/dev.040972

Scambler, P. J. (2010). 22q11 deletion syndrome: a role for TBX1 in pharyngeal and cardiovascular development. *Pediatr. Cardiol.* **31**, 378-390. doi:10.1007/s00246-009-9613-0

Schilling, T. F. and Kimmel, C. B. (1994). Segment and cell type lineage restrictions during pharyngeal arch development in the zebrafish embryo. *Development* **120**, 483-494.

Schneider, R. A. and Helms, J. A. (2003). The cellular and molecular origins of beak morphology. *Science.* **299**, 565-568. doi:10.1126/science.1077827

Sefton, E. M., Piekarski, N. and Hanken, J. (2015). Dual embryonic origin and patterning of the pharyngeal skeleton in the axolotl (Ambystoma mexicanum). *Evol. Dev.* **17**, 175-184. doi:10.1111/ede.12124

Soriano, P. (1999). Generalized lacZ expression with the ROSA26 Cre reporter strain. *Nat. Genet.* **21**, 70-71. doi:10.1038/5007

Srinivas, S., Watanabe, T., Lin, C. S., William, C. M., Tanabe, Y., Jessell, T. M. and Costantini, F. (2001). Cre reporter strains produced by targeted insertion of EYFP and ECFP into the ROSA26 locus. *BMC Dev. Biol.* **1**, 1-8. doi:10.1186/1471-213X-1-4

Tabler, J. M., Rigney, M. M., Berman, G. J., Gopalakrishnan, S., Heude, E., Al-Lami, H. A., Yannakoudiadkis, B. Z., Fitch, R. D., Carter, C., Vokes, S. et al. (2017). Cilia-mediated hedgehog signaling controls form and function in the mammalian larynx. *Elife* **6**, 1-26. doi:10.7554/eLife.19153

Theis, S., Patel, K., Valasek, P., Otto, A., Pu, Q., Harel, I., Tzahor, E., Tajbakhsh, S., Christ, B. and Huang, R. (2010). The occipital lateral plate mesoderm is a novel source for vertebrate neck musculature. *Development* **137**, 2961-2971. doi:10.1242/dev.049726

Tokita, M. and Schneider, R. A. (2009). Developmental origins of species-specific muscle pattern. *Dev. Biol.* **331**, 311-325. doi:10.1016/j.ydbio.2009.05.548

Verzi, M. P., McCulley, D. J., De Val, S., Dodou, E. and Black, B. L. (2005). The right ventricle, outflow tract, and ventricular septum comprise a restricted expression domain within the secondary/anterior heart field. *Dev. Biol.* **287**, 134-145. doi:10.1016/j.ydbio.2005.08.041

Wang, X., Chen, D., Chen, K., Jubran, A., Ramirez, A. J. and Astrof, S. (2017). Endothelium in the pharyngeal arches 3, 4 and 6 is derived from the second heart field. *Dev. Biol.* **421**, 108-117. doi:10.1016/j.ydbio.2016.12.010

Xu, H., Morishima, M., Wylie, J. N., Schwartz, R. J., Bruneau, B. G., Lindsay, E. A. and Baldini, A. (2004). *Tbx1* has a dual role in the morphogenesis of the cardiac outflow tract. *Development* **131**, 3217-3227. doi:10.1242/dev.01174

Yagi, H., Furutani, Y., Hamada, H., Sasaki, T., Asakawa, S., Minoshima, S. and Ichida, F. (2003). Mechanisms of disease Role of TBX1 in human del22q11.2 syndrome. *Lancet* **362**, 1366-1373. doi:10.1016/S0140-6736(03)14632-6